Revised model for the radiation force exerted by standing surface acoustic waves on a rigid cylinder

Shen Liang and Wang Chaohui*

State Key Laboratory of Manufacturing Systems Engineering, Xi'an Jiaotong University, Xi'an, Shaanxi 710049, China and Shaanxi Key Laboratory of Intelligent Robots, Xi'an Jiaotong University, Xi'an, Shaanxi 710049, China

(Received 13 August 2017; revised manuscript received 6 February 2018; published 9 March 2018)

In this paper, a model for the radiation force exerted by standing surface acoustic waves (SSAWs) on a rigid cylinder in inviscid fluids is extended to account for the dependence on the Rayleigh angle. The conventional model for the radiation force used in the SSAW-based applications is developed in plane standing waves, which fails to predict the movement of the cylinder in the SSAW. Our revised model reveals that, in the direction normal to the piezoelectric substrate on which the SSAW is generated, acoustic radiation force can be large enough to drive the cylinder even in the long-wavelength limit. Furthermore, the force in this direction can not only push the cylinder away, but also pull it back toward the substrate. In the direction parallel to the substrate, the equilibrium positions for particles can be actively tuned by changing Rayleigh angle. As an example considered in the paper, with the reduction of Rayleigh angle the equilibrium positions for steel cylinders in water change from pressure nodes to pressure antinodes. The model can thus be used in the design of SSAWs for particle manipulations.

DOI: 10.1103/PhysRevE.97.033103

I. INTRODUCTION

When an object is immersed in a sound field, it is subject to the radiation force caused by the transference of momentum flux from the wave to the body. The transference occurs only under the condition of different acoustic impedances between fluids and the object. Additionally, the body also experiences the Stokes drag force from the suspending medium, which is set in motion by the generation of acoustic streaming. The two forces are the basic mechanism of acoustophoresis [1–5] and have received great attention with the development of microfabrication technologies allowing for integration of ultrasound resonators in microfluidic systems in recent years. In ideal fluids, no mean momentum flux is spent in generating acoustic streaming and, only the radiation force is left acting on the object. Thus, the theoretical development of acoustic radiation force is significant for better applying acoustophoresis in many applications to manipulate particles.

In the past decades, many investigations were conducted in the field of acoustic radiation force. In 1934, King [6] analytically studied the radiation force exerted by plane waves on a rigid sphere suspended in nonviscous fluids in the long-wavelength limit where the radius was far smaller than the wavelength. Based on this seminal contribution, the theoretical study of the radiation force was later extended to take into account viscosity [7,8], temperature [9], elasticity of objects [10], and acoustic streaming [11,12]. Compared with spherical structures, cylindrical objects received less attention in the research of acoustic radiation force. Furthermore, many objects in particle manipulations can be treated as cylindrical structures such as nanowires [13], nanotubes [14], muscle cells [15], and fibers [16]. Therefore, it is meaningful to do extensive research on the radiation force acting on cylinders.

The first theoretical study on acoustic radiation force incident on cylinders dates back to the early work done by Awatani [17], who derived an exact formula for the force due to plane progressive waves on a rigid cylinder with restrictions on the radius. Hasegawa [10] extended the radiation force theory for elastic cylinders and imposed no restrictions on the radiuses by the near-field direction approach. Wu [18] not only calculated the radiation force on a rigid cylinder exposed to plane standing waves, but also did an corresponding experiment to verify the result. Wei and Marston [19–23] developed general theoretical schemes for calculating the radiation force exerted on cylindrical structures in plane standing waves and carried out experiments to verify the schemes. Mitri [24–27] further developed the theory to include absorbing cylinders, viscoelastic cylinders, and coated cylindrical shells.

Previous researchers did much work in the theory of acoustic radiation force on cylinders due to plane traveling waves (PTWs) and plane standing waves (PSWs). As far as the authors know, none of them theoretically studied the radiation force exerted on cylinders in the standing surface acoustic waves (SSAWs). As sketched in Fig. 1(a), the SSAW is formed by two traveling surface acoustic waves (TSAWs), each propagating from the substrate into fluids at an angle (i.e., Rayleigh angle) [28]. The SSAW-based microfluidic techniques have become increasingly popular for the advantages of less requirements, label-free operation, good biocompatibility, compact size, and easy integration with other devices. Great potential has been shown in a wide variety of microfluidic applications such as forcing particles [29], cell enrichment [30], droplets generation [31], sorting particles [32–34], and patterning cells [35–37]. Although the SSAW-based applications receive great attention, the theory used in this field is still based on plane standing waves. As technological development pushes for higher accuracy, and more refined SSAW-based applications, it is extremely necessary to model the radiation force on particles in the SSAW.

*chhw@mail.xjtu.edu.cn

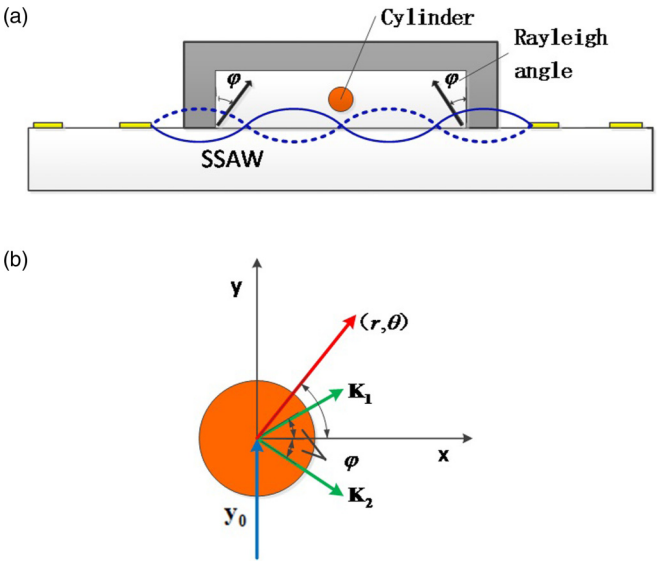

FIG. 1. (a) Two TSAWs generated by a pair of IDTs propagate towards each other. (b) In the microchannel, a cylinder whose axis is perpendicular to the wave vectors of the two TSAWs. A local cylindrical coordinate system (r,θ,z) is built at the instantaneous axis of the cylinder. Additionally, the positive x direction in the global Cartesian coordinate system is normal to the piezoelectric substrate, while the positive y direction is parallel to the substrate.

In this work, a model of acoustic radiation force exerted by the SSAW on a rigid cylinder is revised, where the Rayleigh angle is considered to accurately describe the radiation force. Theoretical study of the model is started from the perturbation theory of the Navier-Stokes equations. The scattering coefficient is calculated to determine the first-order velocity based on the boundary condition. Ignoring viscosity, we compute the radiation force according to the near-field derivation approach, which was applied by Hasegawa [10] in the calculation of the acoustic radiation force stemming from plane waves on an elastic solid cylinder. As Hasegawa, Wei, and Mitri did in previous papers [10,19,24], we introduce the acoustic radiation force function to describe the force. As sketched in Fig. 1(a), when Rayleigh angles equal 0° and 90°, the SSAWs degenerate into PTWs and PSWs, respectively. The analytical expressions obtained from the revised model in the two special Rayleigh angles can reduce to the formulas derived in the corresponding waves. Numerical calculations are carried out to illustrate the Rayleigh angle effects on the radiation force incident on cylinders.

II. THE SOUND FIELD OF THE REVISED MODEL

A. Basic derivation for the sound field

In this model, a rigid cylinder is immersed in ideal fluids. Without incident waves, the motion of ideal quiescent fluids can be described by the following Navier-Stokes equations [38]:

$$\frac{\partial \rho}{\partial t} + \nabla \cdot (\rho \mathbf{u}) = 0, \tag{1a}$$

$$\rho\left(\frac{\partial \mathbf{u}}{\partial t} + \mathbf{u} \cdot \nabla \mathbf{u}\right) = -\nabla p, \tag{1b}$$

where ρ is the fluid density, $\mathbf{u}$ describes the velocity field, and p denotes the pressure.

When an incident wave transports into the bulk medium, additional parts are written based on perturbation theory:

$$\rho = \rho_f + \rho_1 + \rho_2, \tag{2a}$$

$$p = p_f + p_1 + p_2, \tag{2b}$$

$$\mathbf{u} = \mathbf{0} + \mathbf{u}_1 + \mathbf{u}_2, \tag{2c}$$

where we consider the perturbations to first and second order (subscripts 1 and 2, respectively). The stationary parts, denoted by quantities with subscript f, represent the undisturbed properties of fluids. Both the incident and scattering waves are first-order quantities which are extremely small compared with the equilibrium ones.

The first-order quantities are harmonic in time with angular frequency ω, resulting in a zero net force over a period. However, the second-order quantities yield a nonzero value on time averaging, and in fact they contribute to the radiation force. Because the time-averaged second-order quantities are written in terms of the first-order ones, it is necessary to solve linearized Navier-Stokes equations:

$$\frac{\partial \rho_1}{\partial t} + \rho_f \nabla \cdot \mathbf{u}_1 = 0, \tag{3a}$$

$$\rho_f \frac{\partial \mathbf{u}_1}{\partial t} = -\nabla p_1. \tag{3b}$$

In an adiabatic condition, the pressure depends only on density as $p = p(\rho)$. Thus, it can be expressed by $p(\rho) = p_f + (\partial p/\partial \rho)_s \rho_1$ on perturbation expansion. The derivative is related to the speed of sound by $(\partial p/\partial \rho)_s = {c_f}^2$. Consequently, the relation between the first-order pressure and density can be expressed by

$$p_1 = {c_f}^2 \rho_1. \tag{4}$$

Similarly, the time-averaged second-order Navier-Stokes equations are obtained by inserting Eq. (2) into Eq. (1) and averaging all second-order terms on time as

$$\rho_f \nabla \cdot \langle \mathbf{u}_2 \rangle + \nabla \cdot \langle \rho_1 \mathbf{u}_1 \rangle = 0, \tag{5a}$$

$$\left\langle \rho_1 \frac{\partial \mathbf{u}_1}{\partial t} \right\rangle + \rho_f \langle \mathbf{u}_1 \cdot \nabla \mathbf{u}_1 \rangle = -\nabla \langle p_2 \rangle, \tag{5b}$$

where a time-averaged quantity $\langle X \rangle$ represents the quantity $X(t)$ averaged over a full oscillation period τ:

$$\langle X \rangle = \frac{1}{\tau} \int_0^\tau X(t)\, dt. \tag{6}$$

The time-averaged second-order pressure can be derived from Eq. (5) (to learn more details about the derivation, see Ref. [38]):

$$\langle p_2 \rangle = \frac{1}{2\rho_f c_f^2} \langle p_1^2 \rangle - \frac{1}{2} \rho_f \langle \mathbf{u}_1^2 \rangle. \tag{7}$$

B. Evaluating the sound field of the revised model

The SSAW is produced by a pair of identical interdigital transducers (IDTs) fabricated on the piezoelectric substrate. The IDTs generate two TSAWs with the speed of sound c_s

propagating towards each other. When fluids make contact with the surface where the two TSAWs propagate, part of the vibration energy leaks into fluids yielding two longitudinal waves. As sketched in Fig. 1(a), each travels with the speed of sound c_f at the Rayleigh angle [28] φ with respect to the orthogonal:

$$\varphi = \arcsin(c_f/c_s). \tag{8}$$

The TSAWs deliver energy from the substrate to fluids, leading to the wave amplitude decaying exponentially along the fluid-solid interface. However, the microchannel is extremely small for the SSAW-based applications. The attenuation caused by the delivery can thus be neglected in the analysis. Ultimately, the SSAW can be handled as two plane progressing waves with the same amplitude, frequency, and phase, each traveling along the Rayleigh angle φ into fluids (see video in the Supplemental Material [39]). Since the cylinder acted on by the flowing fluids tends to lie parallel to the microchannel, the axis of the cylinder is assumed to be perpendicular to the wave vectors of the two TSAWs. In addition, we assume the length of the cylinder is infinite to exclude the end effects in the derivation.

In ideal fluids, the first-order velocity using the Helmholtz decompositions can be expressed in terms of a scalar potential ϕ:

$$\mathbf{u}_1 = \nabla\phi. \tag{9}$$

The above-mentioned velocity potential consists of the external incident potential ϕ_c and the scattering potential ϕ_s resulting from different acoustic impedances compared with fluids. In the next step, we have to describe the two velocity potentials and further compute the scattering coefficient, and thereby determine the scattering potential.

A cylindrical coordinate system with unit vectors $(\mathbf{e_r}, \mathbf{e}_\theta, \mathbf{e_z})$ is built at the instantaneous axis of the cylinder, as sketched in Fig. 1(b). The SSAW is expanded in a cylindrical partial-wave series with respect to the system as

$$\begin{aligned}\phi_c = \phi_0 \sum_{(n=0)}^{\infty} \epsilon_n (i)^n J_n(k_f r)[2\cos(k_f y_0 \sin\varphi)\cos n\varphi \\ \times \cos n\theta + 2i \sin(k_f y_0 \sin\varphi)\sin n\varphi \sin n\theta] e^{-i\omega t},\end{aligned} \tag{10}$$

where ϕ_0 is the amplitude of scalar velocity potential, k_f is the wave number, and y_0 describes the distance from the center of the cylinder to a pressure antinode. ϵ_n is the Neumann factor, which is defined by $\epsilon_0 = 1$ and $\epsilon_j = 2, j = 1, \ldots, n$, and $J_n(k_f r)$ denotes the Bessel function of the first kind with order n. For more details about the derivation, see Eq. (A1).

In the same manner, the scattered wave potential is given as

$$\begin{aligned}\phi_s = \phi_0 \sum_{(n=0)}^{\infty} \epsilon_n (i)^n s_n H_n(k_f r)[2\cos(k_f y_0 \sin\varphi)\cos n\varphi \\ \times \cos n\theta + 2i \sin(k_f y_0 \sin\varphi)\sin n\varphi \sin n\theta] e^{-i\omega t},\end{aligned} \tag{11}$$

where $H(k_f r)$ is Hankel function of the first kind with order n, and s_n denotes the scattering coefficient which is determined by the boundary condition on the cylinder surface.

The first-order velocity of the cylinder is determined by the instantaneous force caused by hydrodynamic stress. The force can be obtained by integrating the stress on the cylinder surface. In ideal fluids, the tangential stress dependent on viscosity vanishes and only the normal stress is left driving the cylinder,

$$\sigma_{rr} = -i\omega\rho_f \phi, \tag{12}$$

where

$$\begin{aligned}\phi = \phi_0 \sum_{(n=0)}^{\infty} \epsilon_n (i)^n [J_n(k_f r) + s_n H_n(k_f r)][2\cos(k_f y_0 \sin\varphi) \\ \times \cos n\varphi \cos n\theta + 2i \sin(k_f y_0 \sin\varphi)\sin n\varphi \\ \times \sin n\theta] e^{-i\omega t}.\end{aligned} \tag{13}$$

The instantaneous force can be decomposed into two forces F_{1x} and F_{1y} pointing to positive x and y directions, respectively, due to the symmetry of the cylinder. Thus,

$$\begin{aligned}F_{1x} &= a\int_0^{2\pi} \sigma_{rr}|_{r=a} \cos\theta \, d\theta \\ &= 2\omega\rho_f a\pi\phi_0 [J_1(x_f) + s_1 H_1(x_f)]\cos(k_f y_0 \sin\varphi) \\ &\quad \times \cos\varphi e^{-i\omega t},\end{aligned} \tag{14a}$$

$$\begin{aligned}F_{1y} &= a\int_0^{2\pi} \sigma_{rr}|_{r=a} \sin\theta \, d\theta \\ &= 2i\omega\rho_f a\pi\phi_0\epsilon_1 [J_1(x_f) + s_1 H_1(x_f)]\sin(k_f y_0 \sin\varphi) \\ &\quad \times \sin\varphi e^{-i\omega t},\end{aligned} \tag{14b}$$

where a is the radius of the cylinder and $k_f a$ is denoted by x_f.

According to Newton's second law, the forces can also be written as

$$F_{1x} = \rho_p V_p \frac{du_{px}}{dt}, \tag{15a}$$

$$F_{1y} = \rho_p V_p \frac{du_{py}}{dt}, \tag{15b}$$

where ρ_p is the density of the cylinder, and V_p is the unit-length volume of the cylinder.

Substituting Eq. (14) into Eq. (15), we obtain the instantaneous velocities in the x and y directions:

$$\begin{aligned}u_{px} &= 2i\phi_0\epsilon_1 [J_1(x_f) + s_1 H_1(x_f)]\cos(k_f y_0 \sin\varphi) \\ &\quad \times \cos\varphi e^{-i\omega t}/(\bar{\rho}a),\end{aligned} \tag{16a}$$

$$\begin{aligned}u_{py} &= -2\phi_0\epsilon_1 [J_1(x_f) + s_1 H_1(x_f)]\sin(k_f y_0 \sin\varphi) \\ &\quad \times \sin\varphi e^{-i\omega t}/(\bar{\rho}a),\end{aligned} \tag{16b}$$

where ρ_p/ρ_f is denoted by $\bar{\rho}$.

Combining Eq. (9) with Eq. (10), we obtain the normal velocity in fluids:

$$\begin{aligned}u_r|_{r=a} = \phi_0 \sum_{(n=0)}^{\infty} \epsilon_n (i)^n k_f [J_n'(x_f) + s_n H_n'(x_f)] \\ \times [2\cos(k_f y_0 \sin\varphi)\cos n\varphi \cos n\theta \\ + 2i \sin(k_f y_0 \sin\varphi)\sin n\varphi \sin n\theta] e^{-i\omega t}.\end{aligned} \tag{17}$$

In ideal fluids, the appropriate boundary condition on the cylinder surface is the continuity of normal velocity, which means the velocities on the surface inside fluids and the cylinder have to satisfy the following equation:

$$u_r = u_{px}\cos\theta + u_{py}\sin\theta. \tag{18}$$

Substituting Eqs. (16) and (17) into Eq. (18), we obtain the scattering coefficient of each order n:

$$s_n = \begin{cases} -J_n'(x_f)/H_n'(x_f) & (n \neq 1) \\ \frac{\bar{\rho} x_f J_1'(x_f) - J_1(x_f)}{H_1(x_f) - \bar{\rho} x_f H_1'(x_f)} & (n = 1) \end{cases}. \tag{19}$$

Since the scattering coefficient is calculated, any first-order quantity can be determined.

III. EVALUATING THE RADIATION FORCE AND ANALYSIS OF THE RESULTS

In ideal fluids, acoustic radiation force per unit length can be derived by integrating the time-average radiation-stress tensor on the cylinder surface following the procedure in Ref. [10], where the radiation-stress tensor (Π) represents the momentum transferred from the SSAW to the cylinder,

$$\mathbf{F} = -\oint_s \langle \Pi \rangle \, d\mathbf{s} = -\oint_s \langle \mathbf{p_2} + \rho_f \mathbf{u_1}\mathbf{u_1} \rangle d\mathbf{s}, \tag{20}$$

where $\mathbf{F}$ is acoustic radiation force, $d\mathbf{s} = \mathbf{n}ds$ is the elementary area, $\mathbf{n}$ represents the unit vector normal to the surface of the cylinder and pointing outwards, and $\mathbf{p_2}$ denotes a scalar matrix with element p_2. Inserting Eq. (7) into Eq. (20) and rewriting the expression in terms of ϕ, we obtain the radiation force,

$$\mathbf{F} = -\iint_s \left(\left\{ \frac{1}{2}\frac{\rho_f}{{c_f}^2} \left\langle \left[\mathrm{Re}\left(\frac{\partial \phi}{\partial t} \right) \right]^2 \right\rangle - \frac{1}{2}\rho_f \langle |\nabla \mathrm{Re}(\phi)|^2 \rangle \right\} \mathbf{n} + \rho_f \langle (u_n \mathbf{n} + u_t \mathbf{t}) u_n \rangle \right) ds, \tag{21}$$

where $u_n\mathbf{n}$ and $u_t\mathbf{t}$ are the velocities in the normal and tangential directions, respectively. On the circumferential surface, they can also be rewritten as $\mathbf{u}_r$ and $\mathbf{u}_\theta$.

A. Calculation of the radiation force in the positive x direction

In the calculation, the time-averaged unit-length radiation force is decomposed into two forces F_x and F_y pointing to positive x and y directions, respectively, due to the symmetry of the cylinder. The radiation force in the x direction (F_x) including four terms is first evaluated according to Eq. (20),

$$F_x = F_{xr} + F_{x\theta} + F_{xr\theta} + F_{xt}, \tag{22}$$

where each term is given as

$$F_{xr} = -\frac{1}{2} a \rho_f \left\langle \int_0^{2\pi} \left[\mathrm{Re}\left(\frac{\partial \phi}{\partial r} \right) \right]_{r=a}^2 \cos\theta \, d\theta \right\rangle, \tag{23a}$$

$$F_{x\theta} = \frac{\rho_f}{2a} \left\langle \int_0^{2\pi} \left[\mathrm{Re}\left(\frac{\partial \phi}{\partial \theta} \right) \right]_{r=a}^2 \cos\theta \, d\theta \right\rangle, \tag{23b}$$

$$F_{xr\theta} = \rho_f \left\langle \int_0^{2\pi} \left[\mathrm{Re}\left(\frac{\partial \phi}{\partial r} \right) \right]_{r=a} \left[\mathrm{Re}\left(\frac{\partial \phi}{\partial \theta} \right) \right]_{r=a} \sin\theta \, d\theta \right\rangle, \tag{23c}$$

$$F_{xt} = -\frac{a\rho_f}{2{c_f}^2} \left\langle \int_0^{2\pi} \left[\mathrm{Re}\left(\frac{\partial \phi}{\partial t} \right) \right]_{r=a}^2 \cos\theta \, d\theta \right\rangle. \tag{23d}$$

Moreover, F_x can also be written as

$$F_x = Y_{px} S_c E, \tag{24}$$

where $E = \frac{1}{2}\rho_f {k_f}^2 {\phi_0}^2$ denotes the characteristic energy density of the incident wave, $S_c = 2a$ is the unit-length cross-sectional area, and Y_{px} represents acoustic radiation force function [10,40], a dimensionless factor selected for ease of the investigation of the Rayleigh angle effects on the radiation force.

The real and imaginary parts (i.e., α_n and β_n, respectively) of the scattering coefficient s_n are introduced to simplify the expression for Y_{px}. Using Eqs. (A2)–(A5), we obtain a simple and valuable expression for Y_{px},

$$Y_{px} = -\frac{8}{x_f} \sum_{(n=0)}^{\infty} (\alpha_n + \alpha_{n+1} + 2\alpha_n\alpha_{n+1} + 2\beta_n\beta_{n+1}) P_n, \tag{25}$$

where

$$P_n = \cos^2(k_f y_0 \sin\varphi)\cos n\varphi \cos(n+1)\varphi + \sin^2(k_f y_0 \sin\varphi)\sin n\varphi \sin(n+1)\varphi. \tag{26}$$

Compared with the formula derived in PTWs [Eq. (22) in Ref. [10]], our expression for Y_{px} is very similar to it in the form, but every term in our expression is corrected by a factor P_n related to the Rayleigh angle.

The exact solution for the radiation force function is applicable for a rigid cylinder with any size in the SSAW, but including infinite terms resulting in trouble for researchers in the design of SSAWs for particle manipulations. In addition, some SSAW-based applications may fall in the range of $a \ll \lambda_f$ (i.e., $x_f \ll 1$), which means the radius of the cylinder is far smaller than the wavelength in fluids. Note that the range discussed hereby is different from the long-wavelength limit mentioned in other parts where $a \ll \lambda_s$, as most cases appear in the microfluidic systems when operating with the SSAW. Taylor expansion and truncation are applied to simplify Y_{px}, yielding an approximate solution Y_{apx} valid only for $x_f \ll 1$:

$$Y_{apx} = \pi^2 {x_f}^3 \left[\frac{1}{2} + \frac{\bar{\rho}-1}{\bar{\rho}+1} + \frac{1}{2}\left(\frac{\bar{\rho}-1}{\bar{\rho}+1} \right)^2 \right] \times \cos^2(k_f y_0 \sin\varphi) cos\varphi + \frac{\pi^2 {x_f}^3}{2} \left(\frac{\bar{\rho}-1}{\bar{\rho}+1} \right)^2 [\cos^2(k_f y_0 \sin\varphi)\cos\varphi \times \cos 2\varphi + \sin^2(k_f y_0 \sin\varphi)\sin\varphi \sin 2\varphi]. \tag{27}$$

Two special Rayleigh angles are considered to examine the exact expression for the radiation force function Y_{px}. When $\varphi = 0^\circ$, both TSAWs progress in the direction normal to the substrate, which can be regarded as a PTW with double

TABLE I. The speeds of sound of SAWs in two different piezoelectric materials [41,42].

Material	Sound speed c_s (ms^{-1})
$Bi_{12}GeO_{20}$	1640–1800
$KNbO_3$/diamond	12 600

amplitude $2\phi_0$ propagating in the x direction. Substituting $\varphi = 0^\circ$ into Eq. (26) and neglecting the difference in the scattering coefficient, one can find the expression at $\varphi = 0^\circ$ is the same as Eq. (22) in Ref. [10]. In other words, the formula derived in PTWs is recovered when the Rayleigh angle equals 0°. When $\varphi = 90^\circ$, a PSW is formed in the y direction, and Y_{px} is zero, identical to the result predicted by the symmetry principle.

1. Analysis of the calculation results

Before proceeding with the analysis of the Rayleigh angle effects, we have to discuss the practical range for the Rayleigh angle. As given in Eq. (8), the angle is determined by the speeds of sound in the piezoelectric substrate and fluids. We consider two special speeds of sound, namely, the smallest and the largest ones, as far as we know, in both the piezoelectric materials and fluids. The speeds of sound of TSAWs in different piezoelectric materials are listed in Table I and the speeds of sound in different fluids are listed in Table II. We first note the case of air and $KNbO_3$/diamond contributing to the smallest Rayleigh angle (i.e., 1.6°). In the next step, we find the Rayleigh angle could approach 90° in the case of glycol and $Bi_{12}GeO_{20}$. Therefore, the practical range for Rayleigh angle is 1.6°–90°.

The Rayleigh angle effects in Y_{px} are illustrated by curves plotted based on numerical calculations using a Matlab code. When the SSAW formed on the substrate, the wavelength λ_s and wave number k_s are determined by the width of IDTs limited to a reasonable range according to the practical fabrication conditions. The corresponding quantities in fluids λ_f and k_f can be expressed by $\lambda_f = \lambda_s \sin\varphi$ and $k_f = k_s/\sin\varphi$, respectively. The size factor on the substrate defined as $x_s = k_s a$ is introduced to analyze the Rayleigh angle effects in Y_{px}. For ease of investigation, the wavelength of the SSAW is set to $\lambda_s = 0.4$ mm in the following numerical calculations.

In Fig. 2 the value of the dimensionless radiation force Y_{px} obtained from the revised model is plotted as a function of y_0 in the logarithmic scale for four different Rayleigh angles. The case analyzed in the figure describes how a steel cylinder ($\rho_p = 7900$ kg/m^3) with size parameter $x_s = 0.2$ immersed in water ($\rho_f = 997$ kg/m^3) responses to the SSAW. It is observed that Y_{px} is a periodic function with period $\lambda_s/2$ as a result of the term P_n in Eq. (25) with the same period for each order n. In addition, the computation result reveals that at pressure nodes (i.e., $y_0 = 0.1$ or 0.3 mm) the cylinder is also acted on by the

TABLE II. The speeds of sound in two different fluids [9].

Material	Sound speed c_f (ms^{-1})
Air	347.4
Ethylene glycol	1658

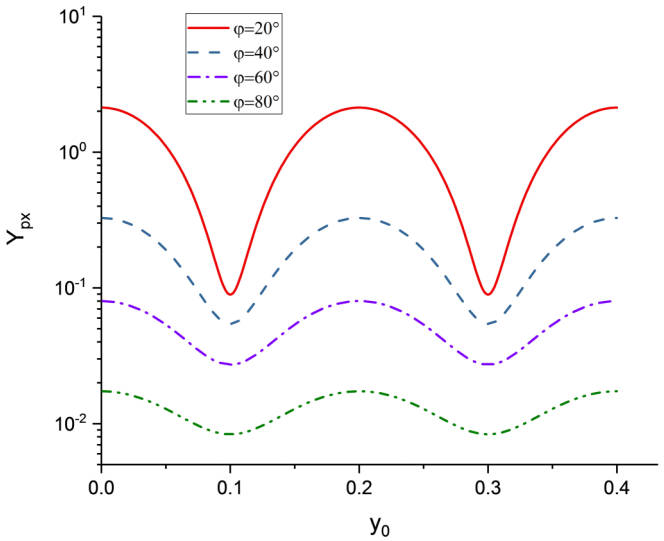

FIG. 2. The value of Y_{px} from Eq. (25) is plotted as a function of y_0 for four different Rayleigh angles (20°, 40°, 60°, and 80°) by considering the case of a steel cylinder ($\rho_p = 7900$ kg/m^3) with fixed size ($x_s = 0.2$) immersed in water ($\rho_f = 997$ kg/m^3).

radiation force stemming from the SSAW, but much smaller than what is estimated at pressure antinodes (i.e., $y_0 = 0$, 0.2, or 0.4 mm). By changing the Rayleigh angle, the curves for Y_{px} can be almost shifted vertically, which means the value of Y_{px} exhibits great dependence on the Rayleigh angle. More specifically, the magnitude of Y_{px} increases with the reduction of Rayleigh angle.

Figure 3 shows the values of Y_{px} over a wide range of size x_f for four different Rayleigh angles using the parameters from

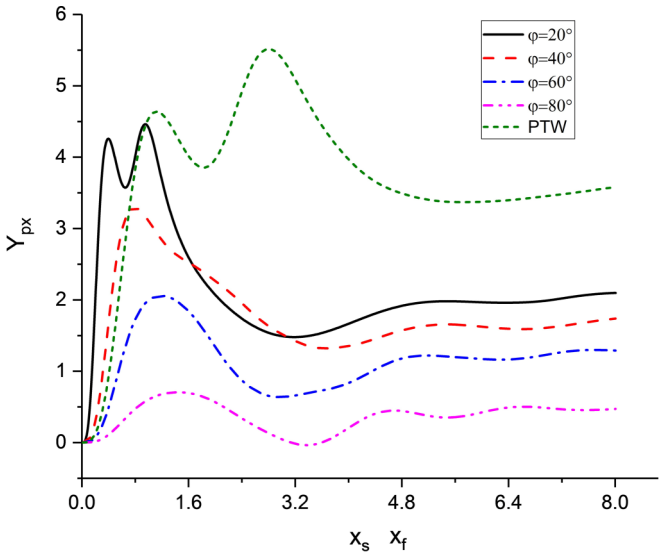

FIG. 3. The value of Y_{px} from Eq. (25) is plotted as a function of x_s for four different Rayleigh angles (20°, 40°, 60°, and 80°) by considering the case of a steel cylinder ($\rho_p = 7900$ kg/m^3) with fixed size ($x_s = 0.2$) immersed in water ($\rho_f = 997$ kg/m^3) and placed at pressure antinodes. In addition, the value of Y_{px} from Eq. (22) in Ref. [10] is plotted by varying x_f for the same case, but in PTWs with the wavelength length being 0.4 mm.

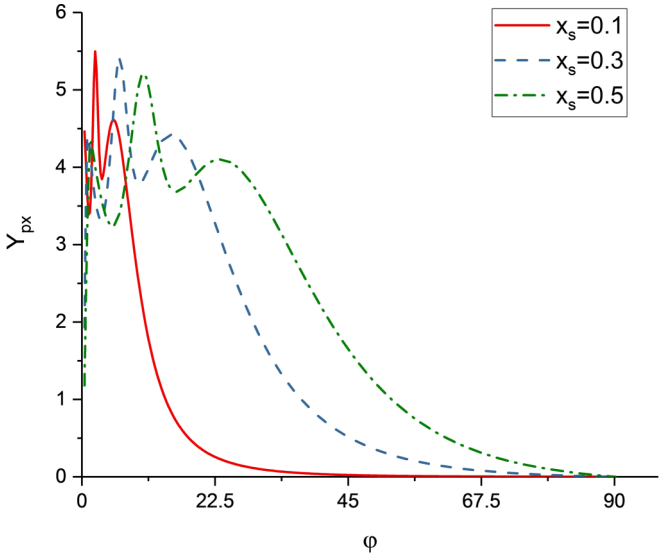

FIG. 4. The value of Y_{px} from Eq. (25) is plotted as a function of φ by considering the case of water ($\rho_f = 997$ kg/m^3) with a suspended steel cylinder ($\rho_p = 7900$ kg/m^3) placed at pressure antinodes for three different size factors ($x_s = 0.1$, 0.3, and 0.5).

the case of a steel cylinder suspended in water and placed at pressure antinodes. Moreover, the situation of PTWs progressing along the x direction is also taken into consideration by plotting the function varying with x_f according to Eq. (22) in Ref. [10], for which the wavelength is set to $\lambda_f = 0.4$ mm. In PTWs, the radiation force turn to be large enough to drive the cylinder, only if x_f approaches or exceeds 1. Conversely, the size restriction for the same purpose in the SSAW can be greatly relaxed by the Rayleigh angle effects. This is expected because for small values of x_s, Y_{px} is proportional to ${x_f}^3$ according to Eq. (27) and x_s is related by $x_s = x_f \sin\varphi$ to x_f. The particle can thus be displaced even in the long-wavelength limit for which $x_s \ll 1$. Inspection of Fig. 3 also reveals that for Rayleigh angle being 80°, there are x_s regions where Y_{px} becomes negative, which means the radiation force is directed toward the substrate on which the SSAW is induced. To our knowledge, this phenomenon has never been discovered before in the research on SSAW-based particle manipulations. With the Rayleigh angle effects the SSAW shows the ability to either trap an object or pull it back toward the source, being a better form of acoustic tweezers.

Using the case of a steel cylinder suspended in water and placed at pressure antinodes, we plot the values of Y_{px} over the whole range of Rayleigh angle (0°–90°) for three different sizes in Fig. 4. The revised model predicts a sharp drop in the value of Y_{px} as a consequence of the term P_n in Eq. (25). This means only the SSAW within a critical Rayleigh angle threshold can exert the radiation force on particles. Furthermore, the threshold value is positively related to the size parameter.

B. Calculation of the radiation force in the positive y direction

Similarly, the acoustic radiation force in the y direction (F_y) also consists of four terms,

$$F_y = F_{yr} + F_{y\theta} + F_{yr\theta} + F_{yt}, \tag{28}$$

where each part is written as

$$F_{yr} = -\frac{1}{2}a\rho_f\left\langle\int_0^{2\pi}\left[\mathrm{Re}\left(\frac{\partial\phi}{\partial r}\right)\right]^2_{r=a}\sin\theta\, d\theta\right\rangle, \tag{29a}$$

$$F_{y\theta} = \frac{\rho_f}{2a}\left\langle\int_0^{2\pi}\left[\mathrm{Re}\left(\frac{\partial\phi}{\partial\theta}\right)\right]^2_{r=a}\sin\theta\, d\theta\right\rangle, \tag{29b}$$

$$F_{yr\theta} = -\rho_f\left\langle\int_0^{2\pi}\left[\mathrm{Re}\left(\frac{\partial\phi}{\partial r}\right)\right]_{r=a}\left[\mathrm{Re}\left(\frac{\partial\phi}{\partial\theta}\right)\right]_{r=a}\cos\theta\, d\theta\right\rangle, \tag{29c}$$

$$F_{yt} = -\frac{a\rho_f}{2{c_f}^2}\left\langle\int_0^{2\pi}\left[\mathrm{Re}\left(\frac{\partial\phi}{\partial t}\right)\right]^2_{r=a}\sin\theta\, d\theta\right\rangle. \tag{29d}$$

Substituting Eq. (29) into Eq. (28) and noting $F_y = Y_{py}S_cE$, we obtain the radiation force function in the y direction. The real and imaginary parts of the scattering coefficient (α_n and β_n, respectively) are introduced to simplify the expression for Y_{py}. Based on Eqs. (A2)–(A5), Y_{py} can be expressed by

$$Y_{yp} = -\frac{4}{x_f}\sum_{(n=0)}^{\infty}(\beta_n - \beta_{n+1} - 2\alpha_n\beta_{n+1} + 2\beta_n\alpha_{n+1})Q_n, \tag{30}$$

where

$$Q_n = \sin(2k_f y_0\sin\varphi)\sin(2n+1)\varphi. \tag{31}$$

Note that every term in Y_{py} is corrected by a factor Q_n related to Rayleigh angle.

In the same way, we apply Taylor expansion and truncation to simplify Y_{py}. An approximate solution Y_{apy} is obtained as

$$Y_{apy} = \pi x_f\left(\frac{2\bar{\rho}}{\bar{\rho}+1}\sin\varphi + \frac{1-\bar{\rho}}{\bar{\rho}+1}\sin 3\varphi\right)\sin(2k_f y_0\sin\varphi). \tag{32}$$

Two special Rayleigh angles ($\varphi = 0°$ and $\varphi = 90°$) are considered to examine the formula Y_{py}. When $\varphi = 0°$, Y_{py} equals zero, which is identical to the result predicted according to the symmetry principle. When $\varphi = 90°$, the SSAW degenerates into a PSW. Y_{py} is the same as Eq. (19) in Ref. [19], which means the formula derived in a PSW is recovered when Rayleigh angle is 90°.

1. Analysis of the calculation results

The value of the dimensionless radiation force [Eq. (30)] caused by the SSAW incident on a steel cylinder with fixed size parameter ($x_s = 0.2$) in water is plotted by varying y_0 in Fig. 5, where five different Rayleigh angles are considered. The value of Y_{py} for each Rayleigh angle is found to show a periodic change as a result of the position-dependent term $\sin(2k_s y_0)$ in Q_n. As mentioned above, the radiation force induced by PSWs can be recovered when Rayleigh angle is 90°. We note that the value of the position-independent form of Y_{py} for steel cylinders illuminated by PSWs in water is positive, which means that steel particles are focused at pressure nodes. Conversely, the particles acted by the SSAW can be expected to move toward pressure antinodes stemming from the Rayleigh

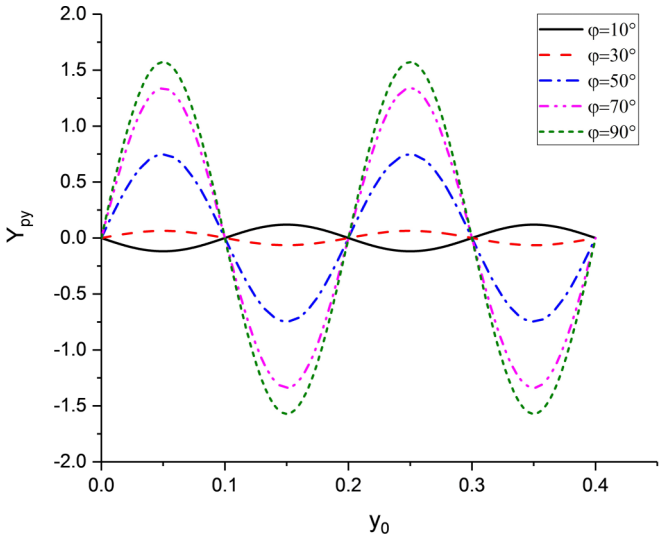

FIG. 5. The value of Y_{py} from Eq. (30) is plotted as a function of y_0 by considering the case of a steel cylinder ($\rho_p = 7900$ kg/m^3) with fixed size ($x_s = 0.2$) surrounded by water ($\rho_f = 997$ kg/m^3) for five different Rayleigh angles (10°, 30°, 50°, 70°, and 90°).

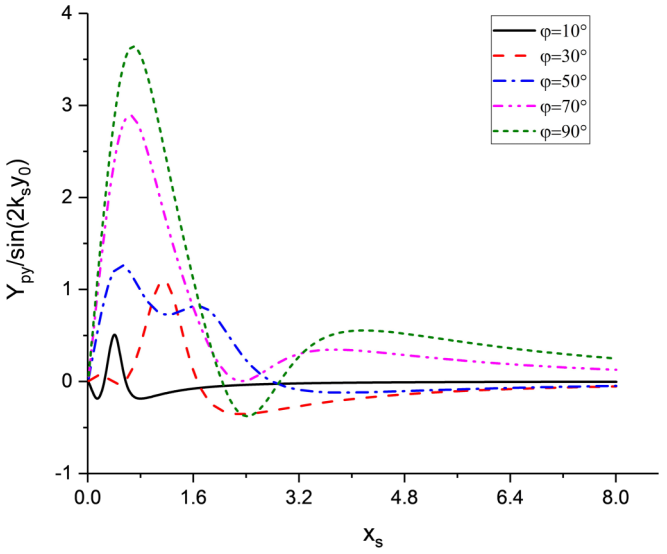

FIG. 6. The value of $Y_{py}/\sin(2k_s y_0)$ from Eq. (30) is plotted as a function of x_s by considering the case of a steel cylinder ($\rho_p = 7900$ kg/m^3) immersed in water ($\rho_f = 997$ kg/m^3) for five different Rayleigh angles (10°, 30°, 50°, 70°, and 90°).

angle corrections according to our revised model, when the Rayleigh angle is 10°. It is known that the equilibrium positions (i.e., pressure nodes or antinodes) are determined by the size of the cylinder and material properties of both fluids and the cylinder, resulting in great restrictions for particle-handling applications. Fortunately, the limit can be broken by the Rayleigh angle effects. In addition, the magnitudes of Y_{py} show remarkable deviation from what predicted according to the theory of PSWs, especially for small Rayleigh angle as depicted in Fig. 5.

Using the parameters from the case of a steel cylinder surrounded by water, we plot the values of $Y_{py}/\sin(2k_s y_0)$ over a wide range of size factor for five different Rayleigh angles in Fig. 6. The value of $Y_{py}/\sin(2k_s y_0)$ exhibits strong dependence on the size factor by a profound relation according to Eq. (30). In addition, the sign of its value also changes with the size factor, which may provide another solution for us to actively tune the equilibrium positions. However, the radius of the cylinder in biophysical or other applications is not allowed to be varied, so as to avoid cell damage or physical properties to change in the particle. Upon comparing the five curves, we note that the magnitude and sign of $Y_{py}/\sin(2k_s y_0)$ are both dependent on Rayleigh angle over the whole range of the size factor considered in the figure. It implies that Rayleigh angle can be used to actively manipulate particles, regardless of their sizes. Inspection of Fig. 7 reveals the same argument that Rayleigh angle plays a dominant role in the magnitude and direction of the radiation force. Furthermore, since $\varphi = \arcsin(c_f/c_s)$, there are two direct ways of tuning the equilibrium positions, i.e., by changing the sound speed of the SSAW or the host medium.

Since the relative density is fixed for the above-mentioned case of a steel cylinder immersed in water, we hereby plot the value of Y_{py} by varying the relative density to avoid loss of generality in Fig. 8, where the size parameter is set to $x_s = 0.5$ and five different Rayleigh angles are considered. It is clearly observed that the value of Y_{py} is a monotonically increasing or decreasing function of $\bar{\rho}$, determined by Rayleigh angle. In addition, the magnitude and sign of Y_{py} show a nontrivial relative density dependence with profound consequences for the radiation force exerted on rigid particles. Since $\bar{\rho} = \rho_p/\rho_f$, the phenomenon predicted by the revised model inspires us to actively tune the equilibrium positions by changing the density of the host medium. Also, note that the densities for common fluids fall in the range of 800–1500 kg/m^3, and for biophysical applications, the host medium is usually water not allowed to be replaced. This may result in a certain restriction for the design of particle-handling devices. However, as discussed above, the

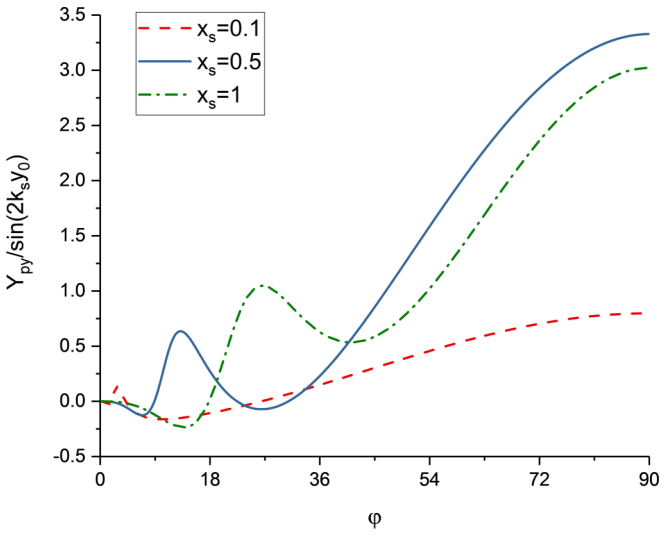

FIG. 7. The value of $Y_{py}/\sin(2k_s y_0)$ from Eq. (30) is plotted as a function of φ by considering a steel cylinder ($\rho_p = 7900$ kg/m^3) immersed in water ($\rho_f = 997$ kg/m^3) for three different size factors ($x_s = 0.1$, 0.5, and 1).

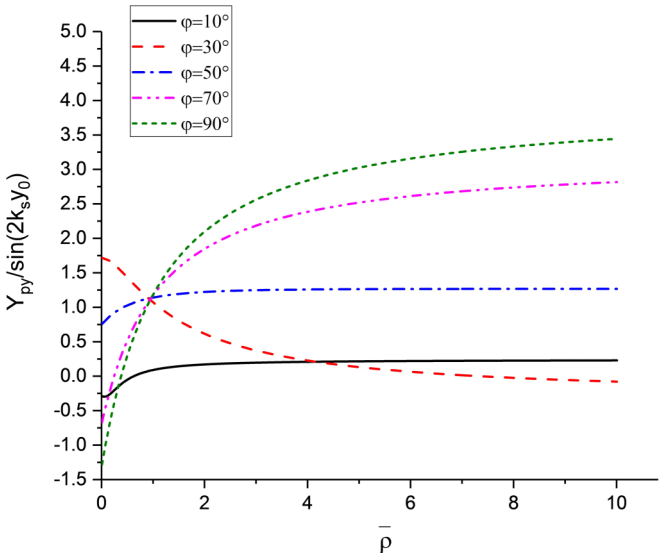

FIG. 8. The value of $Y_{py}/\sin(2k_s y_0)$ from Eq. (30) is plotted as a function of $\bar{\rho}$ for five different Rayleigh angles (10°, 30°, 50°, 70°, and 90°) by fixing the size factor ($x_s = 0.5$).

direction change in the radiation force can be achieved by tuning the Rayleigh angle without any limit in particle size. As depicted in Fig. 8, the condition can be further relaxed leading to the active manipulation valid for any relative densities.

IV. CONCLUSION

In this work, a model for the radiation force caused by the SSAW on a rigid cylinder in inviscid fluids is extended to account for the dependence on the Rayleigh angle. The derivation starts from the perturbation theory of Navier-Stokes equations and is accomplished on the basis of the scattered theory and the near-field derivation approach. The results obtained from plane traveling and standing waves are recovered when Rayleigh angles equal to 0° and 90°, respectively. Numerical calculations are carried out to analyze the Rayleigh angle effects on the radiation force incident on particles.

In the direction normal to the piezoelectric substrate, the revised model reveals that the radiation force can be enlarged by Rayleigh angle, leading to displacing cylinders even in the long-wavelength limit, which is almost impossible for cylinders illuminated by PTWs. Furthermore, the SSAW has the ability to either push the particle away or pull it back toward the sound source, being a better form of acoustic tweezers. In the direction parallel to the substrate, the Rayleigh angle effects play a dominant role in the magnitude and direction of acoustic radiation force. The equilibrium positions (i.e., pressure nodes or antinodes) in PSWs are determined by the shape of the cylinder and material properties of both fluids and the cylinder, resulting in great restrictions for particle-handing applications. The problem can be easily solved in the SSAW by changing Rayleigh angle according to the prediction of the revised model. The model can thus be used in the design of the SSAW-based applications for particle manipulations.

ACKNOWLEDGMENT

This work is supported by the National Natural Science Foundation of China (Grant No. 51575441).

APPENDIX: CYLINDRICAL EXPANSION OF SSAWs AND SPECIAL FUNCTIONS

The SSAW expressed in Sec. II can be derived as the following steps:

$$\begin{aligned}\phi_c &= \phi_0 e^{-i\omega t}\left(e^{i\mathbf{k_1}\cdot(\mathbf{y_0}+\mathbf{r})} + e^{i\mathbf{k_2}\cdot(\mathbf{y_0}+\mathbf{r})}\right)\\ &= \phi_0 e^{i(\mathbf{k_1 y_0})}\sum_{n=0}^{\infty}\epsilon_n (i)^n J_n(kr)\cos n(\theta-\varphi)e^{-\omega t}\\ &\quad + \phi_0 e^{i(\mathbf{k_2 y_0})}\sum_{n=0}^{\infty}\epsilon_n (i)^n J_n(kr)\cos n(\theta+\varphi)e^{-\omega t},\\ &= \phi_0 \sum_{(n=0)}^{\infty}\epsilon_n (i)^n J_n(kr)[2\cos(k y_0\sin\varphi)\cos n\varphi\\ &\quad \times \cos n\theta + 2i\sin(k y_0\sin\varphi)\sin n\varphi\sin n\theta]e^{-i\omega t},\end{aligned} \tag{A1}$$

where $\mathbf{k_1}$ and $\mathbf{k_2}$ are the wave vectors for the two TSAWs, as shown in Fig. 1(a). In Eqs. (23) and (29), the following relations are used:

$$\int_0^{2\pi}\cos n\theta\cos m\theta\cos\theta\, d\theta = \begin{cases}\pi & (n+m=1)\\ \frac{\pi}{2} & (n-m=\pm 1,\\ 0 & n\neq 0, m\neq 0)\\ & \text{otherwise}\end{cases}, \tag{A2a}$$

$$\int_0^{2\pi}\sin n\theta\sin m\theta\cos\theta\, d\theta = \begin{cases}\frac{\pi}{2} & (n-m=\pm 1,\\ 0 & n\neq 0, m\neq 0)\\ & \text{otherwise}\end{cases}, \tag{A2b}$$

$$\int_0^{2\pi}\cos n\theta\sin m\theta\sin\theta\, d\theta = \begin{cases}0 & (n=1, m=0)\\ \pi & (n=0, m=1)\\ \frac{-\pi}{2} & (n-m=1, m\neq 0),\\ \frac{\pi}{2} & (m-n=1, n\neq 0)\\ 0 & \text{otherwise}\end{cases}, \tag{A2c}$$

$$\int_0^{2\pi}\cos n\theta\cos m\theta\sin\theta\, d\theta = 0. \tag{A2d}$$

In Eqs. (A3) and (A4), $F_n(x_f)$ could represent either $J_n(x_f)$ or $N_n(x_f)$:

$$F_n'(x_f) = [F_{n-1}(x_f) - F_{n+1}(x_f)]/2, \tag{A3}$$

$$x_f F_n'(x) = n F_n(x_f) - x_f F_{n+1}(x_f), \tag{A4a}$$

$$x_f F_{n+1}'(x_f) = x_f F_n(x_f) - (n+1)F_{n+1}(x_f). \tag{A4b}$$

The relation between $J_n(x_f)$ and $N_n(x_f)$ can be written as

$$[J_{n+1}(x_f)N_n(x_f) - J_n(x_f)N_{n+1}(x_f)]x_f = 2/\pi. \tag{A5}$$

[1] T. Laurell, F. Petersson, and A. Nilsson, Chip integrated strategies for acoustic separation and manipulation of cells and particles, Chem. Soc. Rev. **36**, 492 (2007).

[2] J. Friend and L. Y. Yeo, Microscale acoustofluidics: Microfluidics driven via acoustics and ultrasonics, Rev. Mod. Phys. **83**, 647 (2011).

[3] Y. Li, J. Y. Hwang, K. K. Shung, and J. Lee, Single-beam acoustic tweezers: A new tool for microparticle manipulation, Acoust. Today **9**, 10 (2013).

[4] K. A. Johnson, H. R. Vormohr, A. A. Doinikov, A. Bouakaz, C. W. Shields, G. P. López, and P. A. Dayton, Experimental verification of theoretical equations for acoustic radiation force on compressible spherical particles in traveling waves, Phys. Rev. E **93**, 053109 (2016).

[5] S. Sepehrirahnama, F. S. Chau, and K.-M. Lim, Effects of viscosity and acoustic streaming on the interparticle radiation force between rigid spheres in a standing wave, Phys. Rev. E **93**, 023307 (2016).

[6] L. V. King, On the acoustic radiation pressure on spheres, Proc. R. Soc. London A **147**, 212 (1934).

[7] M. Settnes and H. Bruus, Forces acting on a small particle in an acoustical field in a viscous fluid, Phys. Rev. E **85**, 016327 (2012).

[8] S. Annamalai, S. Balachandar, and M. K. Parmar, Mean force on a finite-sized spherical particle due to an acoustic field in a viscous compressible medium, Phys. Rev. E **89**, 053008 (2014).

[9] J. T. Karlsen and H. Bruus, Forces acting on a small particle in an acoustical field in a thermoviscous fluid, Phys. Rev. E **92**, 043010 (2015).

[10] T. Hasegawa, K. Saka, N. Inoue, and K. Matsuzawa, Acoustic radiation force experienced by a solid cylinder in a plane progressive sound field, J. Acoust. Soc. Am. **83**, 1770 (1988).

[11] A. A. Doinikov, Acoustic radiation pressure on a rigid sphere in a viscous fluid, Proc. R. Soc. London **447**, 447 (1994).

[12] A. A. Doinikov, Acoustic radiation force on a spherical particle in a viscous heat-conducting fluid. II. Force on a rigid sphere, J. Acoust. Soc. Am. **101**, 722 (1997).

[13] Y. Chen, X. Ding, S.-C. S. Lin, S. Yang, P.-H. Huang, N. Nama, Y. Zhao, A. A. Nawaz, F. Guo, W. Wang *et al.*, Tunable nanowire patterning using standing surface acoustic waves, ACS Nano **7**, 3306 (2013).

[14] Z. Ma, J. Guo, Y. J. Liu, and Y. Ai, The patterning mechanism of carbon nanotubes using surface acoustic waves: The acoustic radiation effect or the dielectrophoretic effect, Nanoscale **7**, 14047 (2015).

[15] J. G. Tidball and T. L. Daniel, Myotendinous junctions of tonic muscle cells: Structure and loading, Cell Tissue Res. **245**, 315 (1986).

[16] S. T. Dubas, P. Kumlangdudsana, and P. Potiyaraj, Layer-by-layer deposition of antimicrobial silver nanoparticles on textile fibers, Colloids Surf. A **289**, 105 (2006).

[17] J. Awatani, Study on acoustic radiation pressure (IV), radiation pressure on a cylinder, Mem. Inst. Sci. Ind. Res. Osaka Univ. **12**, 95 (1955).

[18] J. Wu, G. Du, S. S. Work, and D. M. Warshaw, Acoustic radiation pressure on a rigid cylinder: An analytical theory and experiments, J. Acoust. Soc. Am. **87**, 581 (1990).

[19] W. Wei, D. B. Thiessen, and P. L. Marston, Acoustic radiation force on a compressible cylinder in a standing wave, J. Acoust. Soc. Am. **116**, 2597 (2004).

[20] S. F. Morse, D. B. Thiessen, and P. L. Marston, Capillary bridge modes driven with modulated ultrasonic radiation pressure, Phys. Fluids **8**, 3 (1996).

[21] M. J. Marr-Lyon, D. B. Thiessen, and P. L. Marston, Stabilization of a cylindrical capillary bridge far beyond the Rayleigh-plateau limit using acoustic radiation pressure and active feedback, J. Fluid Mech. **351**, 345 (1997).

[22] M. J. Marr-Lyon, D. B. Thiessen, and P. L. Marston, Passive Stabilization of Capillary Bridges in Air with Acoustic Radiation Pressure, Phys. Rev. Lett. **86**, 2293 (2001).

[23] P. L. Marston and D. B. Thiessen, Manipulation of fluid objects with acoustic radiation pressure, Ann. NY Acad. Sci. **1027**, 414 (2004).

[24] F. G. Mitri, Radiation force acting on an absorbing cylinder placed in an incident plane progressive acoustic field, J. Sound Vib. **284**, 494 (2005).

[25] F. G. Mitri, Theoretical calculation of the acoustic radiation force acting on elastic and viscoelastic cylinders placed in a plane standing or quasistanding wave field, Eur. Phys. J. B **44**, 71 (2005).

[26] F. G. Mitri and Z. E. A. Fellah, Acoustic radiation force on coated cylinders in plane progressive waves, J. Sound Vib. **308**, 190 (2007).

[27] F. G. Mitri, Acoustic radiation force due to incident plane-progressive waves on coated cylindrical shells immersed in ideal compressible fluids, Wave Motion **43**, 445 (2006).

[28] X. Ding, P. Li, S.-C. S. Lin, Z. S. Stratton, N. Nama, F. Guo, D. Slotcavage, X. Mao, J. Shi, F. Costanzo *et al.*, Surface acoustic wave microfluidics, Lab on a Chip **13**, 3626 (2013).

[29] Z. Tengfei, W. Chaohui, N. Dong, J. Weitao, S. Yongsheng, Y. Lei, C. Bangdao, L. Hongzhong, and D. Yucheng, Exploitation of surface acoustic waves to drive nanoparticle concentration within an electrification-dependent droplet, RSC Adv. **4**, 46502 (2014).

[30] Y. Chen, S. Li, Y. Gu, P. Li, X. Ding, L. Wang, J. P. McCoy, S. J. Levine, and T. J. Huang, Continuous enrichment of low-abundance cell samples using standing surface acoustic waves (SSAW), Lab on a Chip **14**, 924 (2014).

[31] S. Li, X. Ding, F. Guo, Y. Chen, M. I. Lapsley, S.-C. S. Lin, L. Wang, J. P. McCoy, C. E. Cameron, and T. J. Huang, An on-chip, multichannel droplet sorter using standing surface acoustic waves, Anal. Chem. **85**, 5468 (2013).

[32] T. Zhu, R. Cheng, S. A. Lee, E. Rajaraman, M. A. Eiteman, T. D. Querec, E. R. Unger, and L. Mao, Continuous-flow ferrohydrodynamic sorting of particles and cells in microfluidic devices, Microfluid. Nanofluid. **13**, 645 (2012).

[33] X. Ding, S.-C. S. Lin, M. I. Lapsley, S. Li, X. Guo, C. Y. Chan, I.-K. Chiang, L. Wang, J. P. McCoy, and T. J. Huang, Standing surface acoustic wave (SSAW) based multichannel cell sorting, Lab on a Chip **12**, 4228 (2012).

[34] L. Ren, Y. Chen, P. Li, Z. Mao, P.-H. Huang, J. Rufo, F. Guo, L. Wang, J. P. McCoy, S. J. Levine *et al.*, A high-throughput acoustic cell sorter, Lab on a Chip **15**, 3870 (2015).

[35] J. Shi, D. Ahmed, X. Mao, S.-C. S. Lin, A. Lawit, and T. J. Huang, Acoustic tweezers: Patterning cells and microparticles using standing surface acoustic waves (SSAW), Lab on a Chip **9**, 2738 (2009).

[36] X. Ding, J. Shi, S.-C. S. Lin, S. Yazdi, B. Kiraly, and T. J. Huang, Tunable patterning of microparticles and cells using standing surface acoustic waves, Lab on a Chip **12**, 2491 (2012).

[37] D. J. Collins, B. Morahan, J. Garcia-Bustos, C. Doerig, M. Plebanski, and A. Neild, Two-dimensional single-cell patterning with one cell per well driven by surface acoustic waves, Nat. Commun. **6**, 8686 (2015).

[38] H. Bruus, Acoustofluidics 7: The acoustic radiation force on small particles, Lab on a Chip **12**, 1014 (2012).

[39] See Supplemental Material at http://link.aps.org/supplemental/10.1103/PhysRevE.97.033103 for the formation process of the SSAW in the microchannel.

[40] F. G. Mitri, Axial time-averaged acoustic radiation force on a cylinder in a nonviscous fluid revisited, Ultrasonics **50**, 620 (2010).

[41] R. G. Pratt, G. Simpson, and W. A. Crossley, Acoustic-surface-wave properties of $Bi_{12}GeO_{20}$, Electron. Lett. **8**, 320 (1972).

[42] S.-i. Shikata, H. Nakahata, A. Hachigo, and M. Narita, Simulation of characteristics of $KNbO_3$/diamond surface acoustic wave, Diam. Relat. Mater. **14**, 167 (2005).